Endothelial LRP1 transports amyloid-β_{1-42} across the blood-brain barrier

Steffen E. Storck,[1] Sabrina Meister,[1] Julius Nahrath,[1] Julius N. Meißner,[2] Nils Schubert,[2] Alessandro Di Spiezio,[3] Sandra Baches,[4] Roosmarijn E. Vandenbroucke,[5,6] Yvonne Bouter,[2] Ingrid Prikulis,[4] Carsten Korth,[4] Sascha Weggen,[4] Axel Heimann,[7] Markus Schwaninger,[3] Thomas A. Bayer,[2] and Claus U. Pietrzik[1]

[1]Institute for Pathobiochemistry, University Medical Center of Johannes Gutenberg University Mainz, Mainz, Germany. [2]Division of Molecular Psychiatry, Department of Psychiatry and Psychotherapy, University Medical Center, Georg-August-University Goettingen, Goettingen, Germany. [3]Institute of Experimental and Clinical Pharmacology and Toxicology, University of Luebeck, Luebeck, Germany. [4]Department of Neuropathology, Heinrich Heine University Duesseldorf, Duesseldorf, Germany. [5]Inflammation Research Center, VIB, Ghent, Belgium. [6]Department of Biomedical Molecular Biology, Ghent University, Ghent, Belgium. [7]Institute for Neurosurgical Pathophysiology, University Medical Center of Johannes Gutenberg University Mainz, Mainz, Germany.

According to the neurovascular hypothesis, impairment of low-density lipoprotein receptor–related protein-1 (LRP1) in brain capillaries of the blood-brain barrier (BBB) contributes to neurotoxic amyloid-β (Aβ) brain accumulation and drives Alzheimer's disease (AD) pathology. However, due to conflicting reports on the involvement of LRP1 in Aβ transport and the expression of LRP1 in brain endothelium, the role of LRP1 at the BBB is uncertain. As global *Lrp1* deletion in mice is lethal, appropriate models to study the function of LRP1 are lacking. Moreover, the relevance of systemic Aβ clearance to AD pathology remains unclear, as no BBB-specific knockout models have been available. Here, we developed transgenic mouse strains that allow for tamoxifen-inducible deletion of *Lrp1* specifically within brain endothelial cells (*Slco1c1-CreER^{T2} Lrp1$^{fl/fl}$* mice) and used these mice to accurately evaluate LRP1-mediated Aβ BBB clearance in vivo. Selective deletion of *Lrp1* in the brain endothelium of C57BL/6 mice strongly reduced brain efflux of injected [^{125}I] $A\beta_{1-42}$. Additionally, in the 5xFAD mouse model of AD, brain endothelial–specific *Lrp1* deletion reduced plasma Aβ levels and elevated soluble brain Aβ, leading to aggravated spatial learning and memory deficits, thus emphasizing the importance of systemic Aβ elimination via the BBB. Together, our results suggest that receptor-mediated Aβ BBB clearance may be a potential target for treatment and prevention of Aβ brain accumulation in AD.

Introduction

Accumulation of amyloid-β (Aβ) in the brain is a key event in Alzheimer's disease (AD) pathogenesis. Recent evidence suggests that in the common sporadic or late-onset forms of AD and in some cases of familiar AD (FAD) elevated Aβ brain levels result from impaired clearance instead of overproduction (1). The most prominent variants of Aβ consist of the first 40 ($A\beta_{1-40}$) and 42 ($A\beta_{1-42}$) amino acids, respectively. The two additional hydrophobic amino acids of $A\beta_{1-42}$ generate a more aggregation-prone and neurotoxic peptide (2). Low Aβ levels within the healthy brain are maintained through degradation, elimination via interstitial fluid (ISF) bulk flow, cerebrospinal fluid (CSF) absorption into the circulatory and lymphatic system, or transport across the blood-brain barrier (BBB) (3, 4). Cell-surface receptor low-density lipoprotein receptor–related protein-1 (LRP1) has been reported to be involved not only in Aβ endocytosis and cerebral degradation (5–7), but also in Aβ transcytosis through the brain endothelium and subsequent systemic elimination via liver, spleen, and kidneys (8).

Aging is the most prominent risk factor for AD. LRP1 expression decreases in total brain and brain capillaries with age (8, 9). Moreover, LRP1 is further reduced in AD (8, 10). Additionally, highly validated genetic risk factors for AD, like the apolipoprotein E (apoE) E4 allele or the gene encoding the phosphatidylinositol-binding clathrin assembly (PICALM), are believed to be linked to reduced clearance of Aβ via LRP1 (11–13). In senile plaques, LRP1 ligands, like apoE, urokinase-type plasminogen activator, tissue plasminogen activator, and lactoferrin, co-deposit with Aβ, all together indicating a loss of LRP1 function in AD (14). Recent studies suggest that transport across the BBB is a major elimination route for brain Aβ (8, 11, 12, 15). Thus, the neurovascular hypothesis of AD states that Aβ accumulation is driven by impairment of Aβ transporters in brain capillaries, resulting in deficient Aβ elimination via the BBB (3, 8, 15, 16).

However, there are conflicting studies showing no or little contribution of LRP1 to Aβ clearance across the BBB (5, 17–20). Due to the lack of appropriate model systems, the role of LRP1 at the BBB and the overall relevance of BBB clearance are insufficiently understood and debated (4, 7). Many Aβ clearance studies make use of LRP1 inhibition through injected antibodies or low-density lipoprotein receptor (LDLR) family antagonists; however, this approach does not allow the specific inhibition of the BBB clearance pathway (21). Global *Lrp1* knockout mice are embryonically lethal (22, 23). Until now, no animal model had been available to study the role of LRP1 at the BBB. Using a brain endothelial–specific Cre-expressing mouse line (24), we generated what we

Authorship note: Sabrina Meister and Julius Nahrath contributed equally to this work.
Conflict of interest: The authors have declared that no conflict of interest exists.
Submitted: January 25, 2015; **Accepted:** October 22, 2015.
Reference information: *J Clin Invest*. 2016;126(1):123–136. doi:10.1172/JCI81108.

believe to be a novel *Lrp1* knockout model. We show that selective deletion of *Lrp1* in brain capillaries strongly reduces Aβ efflux from brain. Using physiological Aβ concentrations, we demonstrate that major amounts of injected radiolabeled Aβ are cleared via endothelial LRP1 across the BBB. In an AD mouse model, deletion of brain endothelial *Lrp1* results in reduced plasma Aβ, elevated soluble brain Aβ, and deficits in spatial memory, underlining the importance of systemic Aβ elimination via the BBB.

Results

Slco1c1-CreER^{T2} × Lrp1$^{fl/fl}$ mice fully excise Lrp1 specifically in brain endothelium. To investigate the function of brain endothelial LRP1, we bred *Lrp1$^{fl/fl}$* mice (25) with tamoxifen-inducible *Slco1c1-CreER^{T2}* mice, producing *Lrp1$_{BE}^{fl/fl}$* mice (24). Upon induction, *Slco1c1-CreER^{T2}* mice have been shown to express Cre recombinase exclusively in brain endothelial cells and choroid plexus epithelial cells but not in other vascular territories. Apart from little recombination in 7% of astrocytes, hardly any Cre is expressed in other cell types of the brain or peripheral organs (24).

Tamoxifen injection in WT mice did not affect *Lrp1* expression (Supplemental Figure 1; supplemental material available online with this article; doi:10.1172/JCI81108DS1). Tamoxifen injection into *Lrp1$_{BE}^{fl/fl}$* mice carrying the *Cre* allele resulted in a full *Lrp1* knockout in brain endothelium (herein referred to as *Lrp1$_{BE}^{-/-}$*), as shown in immunohistochemical staining of cortical brain sections with monoclonal anti-LRP1 11E2 (Figure 1A and Supplemental Figures 2 and 3). Likewise, analysis of lysates revealed the absence of the protein in brain endothelial cells of *Lrp1$_{BE}^{-/-}$* mice (Figure 1B). Full *Lrp1* deletion was also confirmed via PCR analysis (26) on the genomic level (Figure 1C). Having shown full deletion of *Lrp1* in brain endothelium of *Lrp1$_{BE}^{-/-}$* mice, we wanted to verify brain endothelial–specific Cre activity, as reported for *Slco1c1-CreER^{T2}* mice (24). A closer look at the vasculature revealed that CD31-negative cells adjacent to the endothelium that make up the neurovascular unit were positive for LRP1 in *Lrp1$_{BE}^{-/-}$* mice (Figure 1A and Supplemental Figure 3), showing brain endothelial–specific expression of Cre recombinase and no leakage of Cre recombinase in surrounding cells. In both groups, cells surrounding the vasculature showed widespread expression of LRP1. Ubiquitous expression for LRP1 throughout the brain has been reported previously (27). Next, we determined LRP1 abundance in capillary-depleted brain fractions of *Lrp1$_{BE}^{-/-}$* and *Lrp1$_{BE}^{fl/fl}$* mice with different LRP1 antibodies. Neither with the monoclonal N-terminal 11E2 (Supplemental Figure 2) nor with the well-described polyclonal C-terminal antibody 1704 could we see differences in *Lrp1* expression in brain tissue deprived of capillaries (Figure 2). Moreover, we detected LRP1 and different cell markers in cortical brain sections of these mice. NeuN-positive neurons showed strong LRP1 expression in the soma of neurons (Figure 3A), validating high LRP1 expression in neuronal cell bodies as reported previously (28, 29). In addition, the vast majority of glial fibrillary acidic protein–positive (GFAP-positive) astrocytes in *Lrp1$_{BE}^{-/-}$* mice were LRP1 positive (Figure 3B). Little recombination in 7% of astrocytes for this mouse line has been reported before (24). With anti-LRP1 11E2 and a marker for microglia and macrophages (anti-CD11b), we showed costaining of LRP1 and CD11b around vessel-shaped structures in both groups of mice (Figure 3C). CD11b-positive cells away from vessel-shaped structures in both groups of mice showed little colocalization, consistent with previous findings showing weak expression of LRP1 in some glial cells only (27, 29–31). Primary microglia, neurons, and astrocytes isolated from adult *Lrp1$_{BE}^{-/-}$* mice showed abundant LRP1 expression after tamoxifen induction (Supplemental Figure 4). We could not see any effects on the in vivo BBB permeability due to the knockout of *Lrp1* in endothelial cells. Brain permeability for IgG and the low-molecular-weight marker Na-fluorescein did not show differences between genotypes, indicating an intact BBB in vivo (Figure 4).

Deletion of Lrp1 in brain endothelium results in reduced [^{125}I] Aβ$_{1–42}$ transcytosis in vitro. Previously, we have shown that primary brain endothelial cells with inactive LRP1 harboring an NPxYxxL mutation in the endocytosis motif transcytosed significantly less Aβ than WT cells (32). Moreover, several in vivo studies have suggested that LRP1 is involved in Aβ clearance across the BBB (8, 11, 12, 15, 21, 33). However, other studies have failed to see a LRP1 contribution to Aβ BBB clearance in various models (5, 17–19). To understand the discrepancies between previous works, we studied Aβ transport across a *Lrp1*-deficient brain endothelial monolayer in a standard model (5, 32, 34). In the presence of the paracellular marker [^{14}C]-inulin, we investigated [^{125}I] Aβ$_{1–42}$ transport at physiologically relevant concentrations (0.1 nM). The aggregation-prone Aβ$_{1–42}$ variant is the major peptide found in senile plaques and is thought to be a driving agent in AD pathology (2). After 45 minutes, we observed that significant amounts of TCA-precipitable radioactivity, representing intact peptide, were transported across the endothelial monolayer. Moreover, brain endothelial cells lacking LRP1 transcytosed approximately 50% less [^{125}I] Aβ$_{1–42}$ than brain endothelial cells isolated from littermate controls harboring the *Lrp1* allele (Figure 5A). Then, we investigated a range of different physiologically relevant Aβ concentrations to validate our findings. We used Aβ concentrations ranging from 0.05 nM, normally found in plasma of healthy individuals (15), to 5 nM, corresponding to elevated Aβ levels in brains of patients with AD and AD animal models (15). At all concentrations studied, we could verify our previous findings, showing that *Lrp1* knockout endothelial cells transcytosed significantly less [^{125}I] Aβ$_{1–42}$ than control endothelial cells (Figure 5B). Interestingly, we observed the increasing contribution of LRP1 in receptor-mediated transcytosis of [^{125}I] Aβ$_{1–42}$ at rising Aβ concentrations. This demonstrated that LRP1, with an extremely fast endocytosis rate (35), has a major function as an Aβ clearance receptor in endothelial cells.

Deletion of Lrp1 in brain endothelium impairs Aβ efflux from brain. After verification of LRP1-mediated Aβ transcytosis, we aimed to study the role of endothelial LRP1 in vivo with the brain efflux index method (8, 11, 12, 15). It has been shown that clearance rates for [^{125}I]-labeled Aβ and unlabeled Aβ are virtually identical (11). Therefore, pathophysiological concentrations of [^{125}I]-radiolabeled, monomeric Aβ$_{1–42}$ (5.14 nM) were injected simultaneously with 40 μCi/ml [^{14}C]-inulin into ISF of *Lrp1$_{BE}^{fl/fl}$* and *Lrp1$_{BE}^{-/-}$* littermates. [^{14}C]-inulin is not actively cleared or retained in the brain and acts as a reference marker of ISF bulk flow. We injected [^{14}C]-inulin and [^{125}I]Aβ$_{1–42}$ into the caudate putamen, distant from the ventricular system, to promote BBB

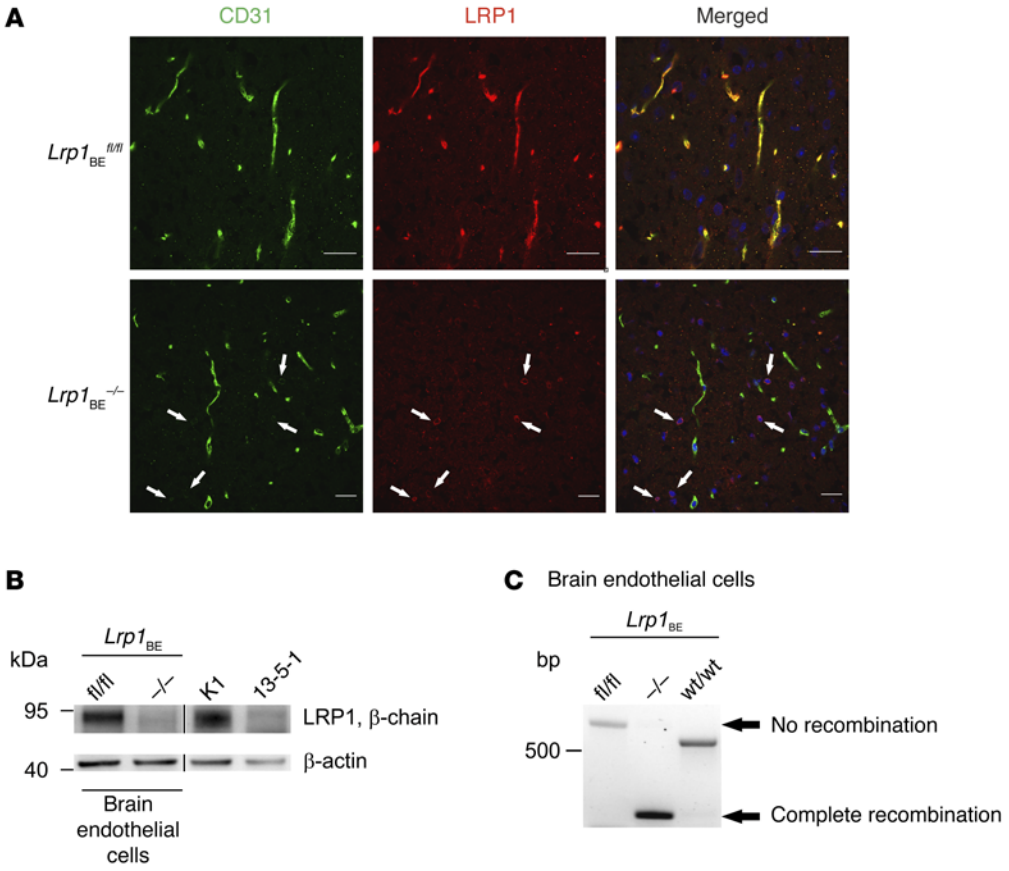

Figure 1. Full deletion of *Lrp1* in *Lrp1*$_{BE}^{-/-}$ mice. (**A**) Immunofluorescent staining for endothelial marker CD31 and LRP1 in cortical brain sections demonstrated complete knockout of *Lrp1* in brain endothelium of *Lrp1*$_{BE}^{-/-}$ animals, while *Lrp1* expression in surrounding cells remained unaffected (white arrows). DRAQ5 was used to stain cell nuclei. Scale bar: 20 μm. (**B**) Immunostaining in isolated endothelial cells showed knockout of *Lrp1* in *Lrp1*$_{BE}^{-/-}$ mice. Primary cortical endothelial cell and control lysates of LRP1-expressing CHO cells (K1) and LRP1 knockout (13-5-1) cells were analyzed on the same Western blot but rearranged for clearer presentation. An anti–β-actin immunoblot is shown as a loading control. (**C**) PCR analysis revealed complete Cre-mediated excision of the loxP-flanked *Lrp1* allele in brain endothelium. Endothelial genomic DNA was used for PCR detecting the WT (WT/WT, 507 bp), the loxP-flanked (*fl/fl*, 541 bp), and the excised allele (–/–, 325 bp) simultaneously in one reaction. Data show representative results from experiments performed in triplicate.

clearance across capillaries instead of CSF-blood barrier clearance across the choroid plexus. First, we determined the time frame for linear [^{125}I] Aβ efflux, since low concentrations of [^{125}I] Aβ are rapidly cleared (36). Precipitating brain radioactivity at designated time points after Aβ injection, we observed that at each time point *Lrp1*$_{BE}^{-/-}$ mice retained more [^{125}I] Aβ$_{1-42}$ than *Lrp1*$_{BE}^{fl/fl}$ mice (Figure 6A). Within the first 20 minutes, Aβ was cleared in a linear manner, with 47.7% more clearance in *Lrp1*$_{BE}^{fl/fl}$ mice studied 15 minutes after injection (Figure 6A). The paracellular marker [^{14}C]-inulin was cleared in a slow, passive, and equal manner in both groups, demonstrating an intact BBB (Figure 6B). Importantly, both tracers were hardly detectable in CSF, with no differences among the groups (Figure 6, D and E). This implicated that the low concentrations of Aβ injected into the caudate putamen were mostly eliminated by rapid clearance across the microvessels and not by clearance from the ISF into the CSF. The amounts of tracers found in the plasma were low due to rapid systemic body clearance (8). As 15 minutes after microinjection [^{125}I] Aβ efflux was linear, we calculated the contribution of the BBB to Aβ clearance contribution in *Lrp1*$_{BE}^{-/-}$ and *Lrp1*$_{BE}^{fl/fl}$ mice. We detected that rapid BBB transport was reduced by about 48% in *Lrp1*$_{BE}^{-/-}$ mice (Figure 6C), whereas clearance through slow ISF bulk flow, a minor component of Aβ brain efflux (8), was not altered (Figure 6B). By subtracting BBB-mediated clearances of *Lrp1*$_{BE}^{-/-}$ animals from *Lrp1*$_{BE}^{fl/fl}$ animals, we calculated the amount of Aβ clearance mediated by brain vasculature LRP1. We found that at 5.14 nM [^{125}I] Aβ$_{1-42}$, 47.5% of Aβ$_{1-42}$ BBB clearance was mediated by brain endothelial LRP1. Therefore, brain endothelial LRP1-mediated clearance accounted for approximately 27% of total Aβ$_{1-42}$ clearance (Figure 6F) at the Aβ concentration used in the study. As *Lrp1* excision is restricted to the brain endothelium, clearance by brain vasculature LRP1 could also be determined by subtracting total clearance in *Lrp1*$_{BE}^{-/-}$ mice from total clearance in *Lrp1*$_{BE}^{fl/fl}$ mice. Both calculations revealed that, at pathophysiological concentrations, about 27% of total Aβ$_{1-42}$ clearance is mediated by LRP1 in the brain endothelium, demonstrating the importance of systemic clearance across the BBB. In order to clear about 70% of injected [^{125}I] Aβ$_{1-42}$, mice lacking *Lrp1* in brain endothelium needed about 4 times longer than control mice (Figure 6A, 60 minutes for *Lrp1*$_{BE}^{-/-}$ versus 15 minutes for *Lrp1*$_{BE}^{fl/fl}$), stressing the importance of endothelial LRP1 in rapid Aβ clearance. Interestingly, 30 minutes after CNS injection, Aβ brain retention in both groups approximated a respective plateau, with reduction (about 44%) of Aβ brain retention in brains of *Lrp1*$_{BE}^{fl/fl}$ animals, even 3 hours after injection of these small amounts of tracers (Figure 6A). This suggested that approximately 44% of the low nM Aβ pool in mice still present after 3 hours could only be cleared when LRP1 was present in brain endothelium.

To investigate the importance of LRP1 on BBB Aβ clearance in a well-established mouse AD model, we crossed the *Lrp1*$_{BE}^{fl/fl}$ mice with 5xFAD mice. These mice express 5 FAD mutations under *Thy-1* promotor control to increase overall Aβ$_{1-42}$ production in the brain (37). Through deletion of brain endothelial *Lrp1* in 5xFAD mice we could study Aβ transport without the need to inject radiolabeled peptides.

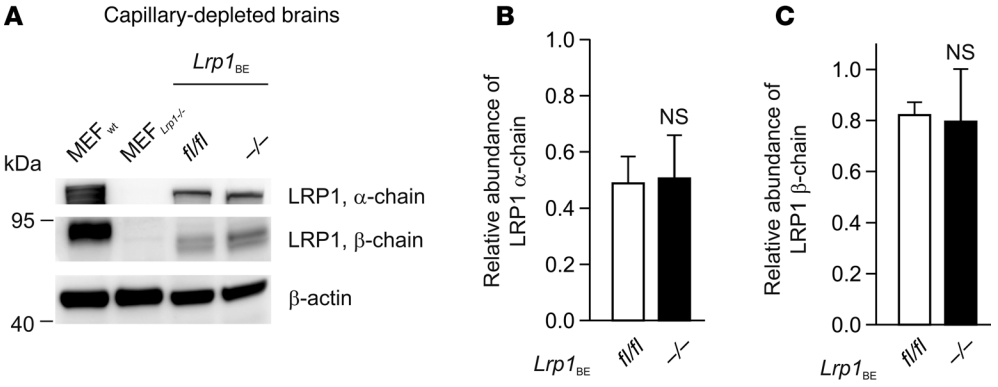

Figure 2. No difference in *Lrp1* expression in capillary-depleted brain fractions of $Lrp1_{BE}^{-/-}$ and $Lrp1_{BE}^{fl/fl}$ mice. (**A**) Immunostaining of LRP1 α chain and β chain in brain fractions deprived of capillaries. An anti–β-actin immunoblot is shown as a loading control. MEF, mouse embryonic fibroblast. (**B** and **C**) Quantification of relative abundance of (**B**) LRP1 α chain and (**C**) LRP1 β chain in brain fractions deprived of capillaries. Data show representative results of 3 to 5 mice per group from experiments performed in triplicate (mean ± SEM). For statistical analyses, unpaired *t* test was used.

We determined Aβ efflux and brain retention in 7-month-old 5xFAD $Lrp1_{BE}^{fl/fl}$ and 5xFAD $Lrp1_{BE}^{-/-}$ mice. 5xFAD $Lrp1_{BE}^{-/-}$ mice showed reduced plasma levels of both $Aβ_{1-40}$ and $Aβ_{1-42}$ associated with reduced Aβ transport out of the brain (Figure 7, A, D, and E). In line with these data, we found significantly higher levels of soluble Aβ in 5xFAD $Lrp1_{BE}^{-/-}$ brains, consistent with impaired transport of Aβ out of the brain (Figure 7, B, F, and G). Soluble Aβ levels were elevated about 2.5-fold for $Aβ_{1-42}$ and about 3.7-fold for $Aβ_{1-40}$ in 5xFAD $Lrp1_{BE}^{-/-}$ mice. Insoluble $Aβ_{1-42}$ levels showed a trend toward higher levels in 5xFAD $Lrp1_{BE}^{-/-}$ mice, with higher variations in individual mice (Figure 7, C, H, and I). Therefore, we determined the absolute Aβ levels in 5xFAD $Lrp1_{BE}^{-/-}$ mice and littermates via ELISA. Reflecting the immunoprecipitation data, 7-month-old 5xFAD mice had significantly higher soluble Aβ levels (approximately 4.8-fold for $Aβ_{x-40}$ and 3.1-fold for $Aβ_{x-42}$) and insoluble $Aβ_{x-40}$ levels (approximately 2.0-fold change) when LRP1 was absent in brain endothelium (Figure 7, L and M). Again, there was a trend toward higher insoluble $Aβ_{x-42}$ levels that did not reach statistical significance (Figure 7L). Plaque load quantification mirrored the data collected from prior measurements and showed no significant difference in plaque load in the hippocampus (Figure 7, J and K), cortex, or subiculum (Supplemental Figure 5). In AD, activated astrocytes and microglia play an important role in clearing Aβ deposits by triggering phagocytic uptake (38, 39). Both AD models showed reactive astrocytes and microglia in the hippocampus (Figure 8). However, we found no significant difference in Iba1 or GFAP immunoreactivity between 5xFAD $Lrp1_{BE}^{-/-}$ and 5xFAD $Lrp1_{BE}^{fl/fl}$ mice.

All together, the collected data from two different in vivo models indicated that brain endothelial LRP1 substantially regulates the soluble brain Aβ levels and that LRP1-mediated transport across the BBB is a major pathway of Aβ clearance.

Differential binding affinity of LRP1 to $Aβ_{1-40}$ and $Aβ_{1-42}$ species. There are several studies showing higher binding affinity of LRP1 to $Aβ_{1-40}$ than to $Aβ_{1-42}$ (11, 15). Since we observed that brain endothelial LRP1 mediated approximately 50% of $Aβ_{1-42}$ transport across the BBB in vivo and in vitro, we analyzed $Aβ_{1-42}$/$Aβ_{1-40}$ ratios in brains and plasma of 5xFAD $Lrp1_{BE}^{-/-}$ mice and littermate controls. 5xFAD mice showed a preferential generation of $Aβ_{1-42}$ over $Aβ_{1-40}$ due to the mutations in amyloid precursor protein (*APP*) and presenilin-1 (37). In 7-month-old 5xFAD $Lrp1_{BE}^{fl/fl}$ animals, both soluble and insoluble $Aβ_{1-42}$/$Aβ_{1-40}$ brain ratios were significantly elevated (Figure 9), suggesting that LRP1 preferentially clears $Aβ_{1-40}$, even when $Aβ_{1-42}$ is of higher abundance. Additionally, the plasma $Aβ_{1-42}$/$Aβ_{1-40}$ ratios in 5xFAD $Lrp1_{BE}^{fl/fl}$ animals were lowered by about the same fold (Figure 9). This demonstrates that LRP1 preferentially binds $Aβ_{1-40}$ when available, confirming previous findings showing a differential affinity of LRP1 to the two Aβ variants (15).

Brain endothelial LRP1 deficiency exacerbates Aβ-dependent cognitive deficits. Next, we investigated how brain endothelial LRP1 deficiency affects AD-related behavior by examining spatial learning and memory (40, 41). We used three different tests to examine motor deficits, string suspension, inverted grip, and balance beam, and found that no mice in any tested group showed abnormalities (Supplemental Figure 6). The ability of vision of the mice was tested by visual placing (42) before mice entered the Morris water maze. The Morris water maze is a particularly sensitive test to examine age-related memory impairments in AD mice. Previously, it has been shown that 5xFAD mice display AD-like memory deficits at 12 months of age (43). Same-aged WT mice, however, did not show these deficits. As we saw that knockout of *Lrp1* in the brain cerebrovasculature of 5xFAD mice severely elevated the soluble brain Aβ levels, we investigated whether 5xFAD $Lrp1_{BE}^{fl/fl}$ mice displayed memory deficits early and examined spatial learning and memory at 7 months of age. Spatial learning tests in 5xFAD $Lrp1_{BE}^{-/-}$ mice after acquisition training showed significantly higher escape latencies on days 3, 4, and 5 compared with those of the rest of the groups (Figure 10A). Swimming speeds did not differ among groups (Figure 10B). These results suggest that spatial learning is impaired in 5xFAD $Lrp1_{BE}^{-/-}$ mice. The probe trial for monitoring spatial reference memory revealed that 3 of 4 groups, including 5xFAD $Lrp1_{BE}^{fl/fl}$ mice, displayed a significant preference for the target quadrant, whereas no quadrant preference was found for 5xFAD $Lrp1_{BE}^{-/-}$ mice (Figure 10, C and D). Swimming speeds did not differ among groups (Figure 10E). In summary, the results illustrated that endothelial-specific *Lrp1* knockout in 5xFAD mice and, therefore, reduced clearance of Aβ peptides induced an impairment of both spatial learning and spatial reference memory.

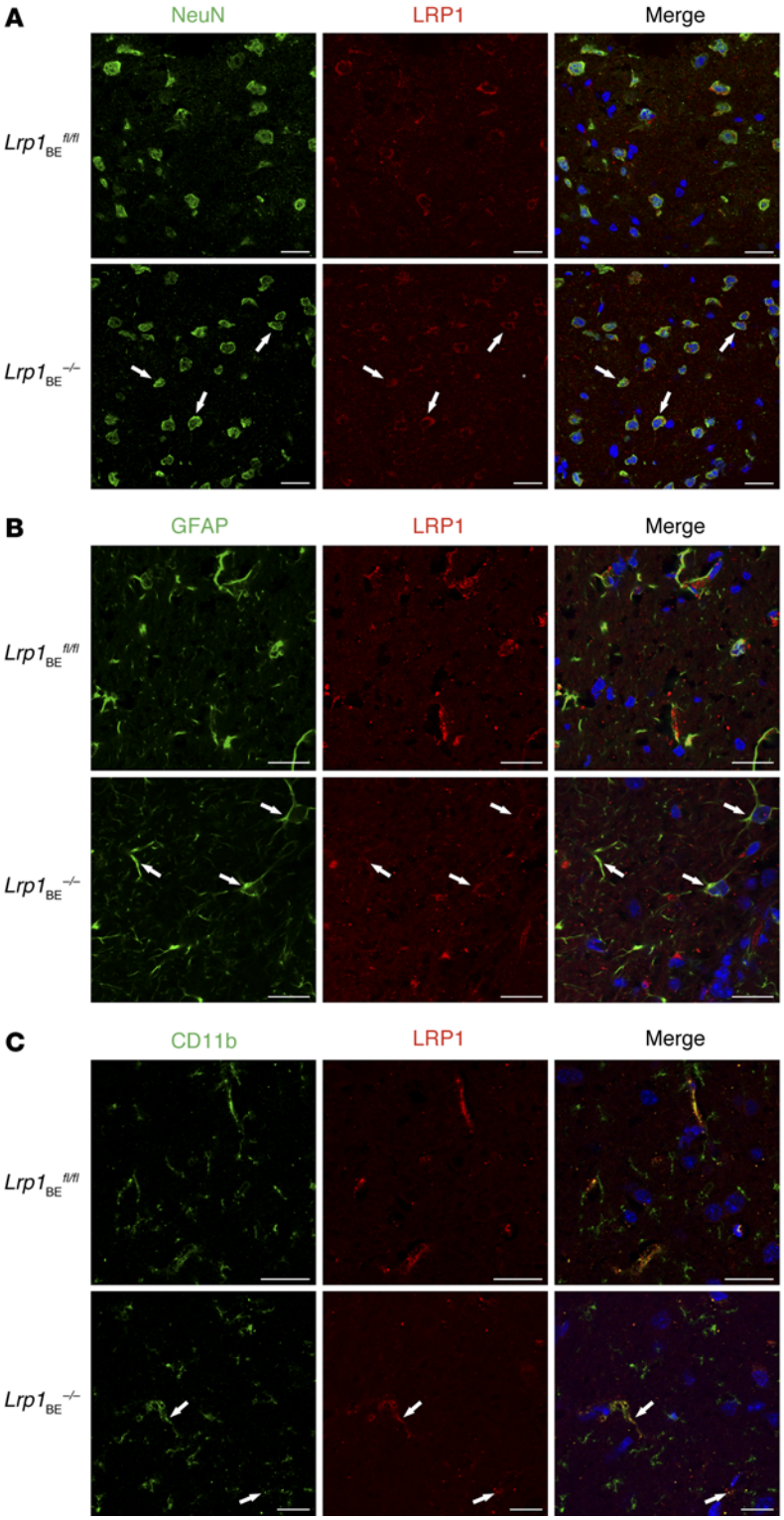

Figure 3. Brain endothelial–specific deletion of *Lrp1* in $Lrp1_{BE}^{-/-}$ mice. Immunofluorescent staining in cortical brain sections for LRP1 and (**A**) NeuN-positive neuronal cells, (**B**) GFAP-positive astrocytes, and (**C**) CD11b-positive microglia and macrophages to determine potential recombination in macrophages/microglia, neurons, and astrocytes revealed no differences between genotypes. Scale bar: 20 μm. Data show representative results from experiments performed in triplicate.

Discussion

Epidemiological studies have shown that risk factors for vascular diseases, like diabetes mellitus, atherosclerosis, stroke, hypertension, and microvessel pathology, are closely associated with AD (3, 44, 45). Moreover, basically all risk factors for AD have vascular components that reduce cerebral perfusion, affecting brain clearance of toxins such as Aβ, providing further evidence for the importance of cerebrovasculature function in the healthy brain (2, 45). The knockdown of LRP1 in the endothelium of zebrafish has resulted in reduced blood flow and demonstrated the importance of LRP1 in vasculogenesis (46). The neurovascular hypothesis suggests that impaired Aβ clearance by BBB transporters leads to rising Aβ brain levels and the initiation and progression of AD. Recently, it has been shown that genetic risk factors for AD are linked to reduced clearance of Aβ via LRP1 (12, 13). However, controversial findings from different groups and the lack of appropriate models to study BBB transporters have created growing ambiguity in the field (8, 11, 12, 15, 17–19, 47). Previous reports have shown no contribution for LRP1 to transcytosis of Aβ in different BBB models (5, 18, 19), and research teams have doubted that the expression of *Lrp1* in brain endothelium is sufficient to mediate substantial Aβ clearance (7, 28, 48, 49). Here, with the first brain endothelial–specific *Lrp1* knockout model to our knowledge, we show that LRP1 in brain endothelial cells is a key transporter mediating Aβ efflux out of the brain. Deletion of *Lrp1* in brain endothelium in an AD mouse model enhances Aβ accumulation and leads to AD-related behavioral deficits.

To our knowledge, Cre recombinase under the control of endothelial cell–specific promoters has not been used to address the role of brain endothelium in Aβ clearance. Previous studies have highlighted the importance of Aβ clearance by cellular degradation in neurons (6), astrocytes (39), microglia cells (38), and vascular smooth muscle cells (7). Numerous studies have tried to show the relevance of BBB contribution to Aβ clearance in vivo; however, they have failed to specifically inhibit brain vasculature LRP1 or have neglected the role of Aβ degradation within the brain (8, 11, 15, 33). Here, for what we believe to be the first time, a BBB-specific knockout mouse was used to evaluate the relevance of Aβ BBB clearance via LRP1.

We studied whether clearance of AD pathology–driving $Aβ_{1-42}$ is affected in $Lrp1_{BE}^{-/-}$ mice. Using physiological Aβ concentrations, we observed that half of the BBB clearance is mediated by brain endothelial LRP1 in various model systems. In vivo, plasma Aβ levels in 5xFAD mice were significantly reduced and soluble brain levels were significantly elevated when LRP1 was absent in brain

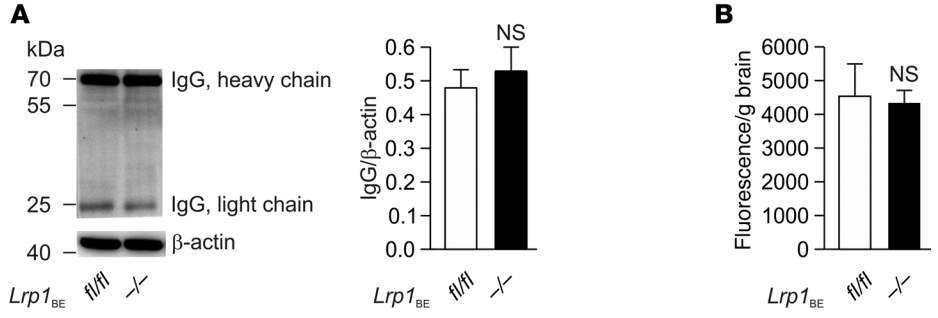

Figure 4. Deletion of *Lrp1* in *Lrp1*$_{BE}^{-/-}$ mice does not affect BBB integrity. (**A**) Brain IgG extravasation and (**B**) fluorescein permeability studies in *Lrp1*$_{BE}^{fl/fl}$ (n = 5) and *Lrp1*$_{BE}^{-/-}$ (n = 8) mice showed no effect of *Lrp1* knockout on BBB permeability in vivo. (**A**) Brain lysates were analyzed by Western blotting and normalized to β-actin. (**B**) Mice were injected with Na-fluorescein, and fluorescence intensity of brain homogenates (emission at 519 nm, excitation at 488 nm) was normalized to brain weight. Data represent mean ± SEM. For statistical analyses, unpaired t test was used.

endothelium. When injecting low nM [^{125}I] Aβ_{1-42} concentrations in mice, we found no significant amount of radioactivity in the CSF, showing that the small amounts of injected Aβ are rapidly cleared via the BBB and that a minor amount of injected Aβ is cleared via bulk flow as also observed by previous studies (8, 11, 12). We found that approximately 48% of BBB transport is mediated by LRP1. This is in line with previous studies showing that Aβ brain efflux can be reduced to approximately 50% by coinjecting LRP1 antibodies or antagonists (8, 21). Moreover, it has been shown that deletion of very LDLR (VDLDR) and LDLR genes did not significantly affect Aβ brain clearances, suggesting a minor importance of other LDL receptors in Aβ brain-to-blood transport (15). Besides, our data collected from the 180-minute time point suggest that brain endothelial LRP1 is able to clear low nM Aβ pools that can only be cleared by the LRP1. Having shown that LRP1 in brain endothelium in vivo mediates approximately 27% of total Aβ clearance at pathophysiological levels, LRP1 at the BBB seems to be a key player in AD pathology. In addition, the in vitro transport studies revealed a substantial contribution of LRP1 in Aβ transcytosis. The data furthermore suggest that, at elevated Aβ concentrations, like during the progression of AD, the importance of Aβ clearance by fast endocytic receptor LRP1 is crucial. While, at picomolar concentrations, the contribution of LRP1-mediated clearance was 49.2% (0.1 nM Aβ), it increased with rising Aβ concentrations to 65.4% at 5 nM Aβ. This could be due to the high Aβ-binding capacity and the fast endocytosis rate of LRP1. It has been shown that, at 5 nM, Aβ binding to LRP1 is not yet saturated (50, 51). Moreover, with an endocytosis rate up to 16 times faster than that of other Aβ receptors, such as VDLDR or LDLR (12, 35), LRP1 may outperform other receptors in Aβ clearance, especially at higher concentrations. Additionally, in the 5xFAD mouse model, we could collect in vivo data on the importance of LRP1 in clearance at higher Aβ levels. Aβ brain levels in 5xFAD mice rise with age (37). In 7-month-old 5xFAD *Lrp1*$_{BE}^{-/-}$ animals, the plasma levels for both Aβ_{1-40} and Aβ_{1-42} are strongly reduced and the brain levels highly elevated, each by more than 50%. This strong effect is probably not solely the result of deficient BBB and CSF-blood clearance in these animals but could also be due to the predominant importance of LRP1 at rising Aβ levels in aging animals.

Previous studies have shown higher binding affinity of LRP1 to Aβ_{1-40} and faster clearance of this variant than of Aβ_{1-42} (11, 15). We confirmed these findings in 5xFAD *Lrp1*$_{BE}^{-/-}$ mice in vivo. When measuring the Aβ_{1-42}/Aβ_{1-40} ratio in 5xFAD mice, we saw that both Aβ variants were cleared by LRP1 but noticed preferential clearance of Aβ_{1-40}. This binding affinity difference could lead to fatal consequences in patients. When LRP1 expression decreases during aging and in AD (8, 10), fewer receptors will not only cause rising Aβ accumulation in the brain, but will preferentially clear less toxic Aβ_{1-40} and therefore cause a shift in the Aβ_{1-42}/Aβ_{1-40} ratio, leading to higher concentrations of aggregation-prone Aβ_{1-42}. The binding affinity results, as well as the predominant importance of LRP1 at elevated Aβ concentrations, support the idea that maintaining steady Aβ clearance at the BBB by LRP1 could be a potential target for treatment of age-related neurological disorders (51).

We are aware that there are conflicting findings on LRP1 in previous studies. These results might be due to Aβ injections at concentrations beyond physiological relevance into different brain regions (17, 18, 52) or the use of epithelial cells, such as MDCK and CHO cells (5, 19), for in vitro studies. Cell-specific functions of receptors have been reported for other members of the LDLR family (53), so the function of LRP1 might be dependent on cell type and polarization state, as suggested before (21, 32).

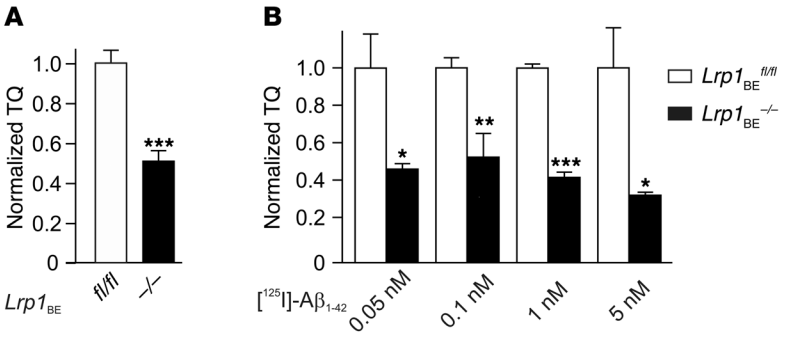

Figure 5. LRP1 in brain endothelial cells substantially contributes to [^{125}I] Aβ_{1-42} transcytosis in vitro. [^{125}I] Aβ_{1-42} transport across the primary mouse brain capillary endothelial cell monolayer was studied in the presence of 1 μCi/ml [^{14}C]-inulin to determine the transcytosis quotient (TQ). Transcytosis was analyzed in the brain-to-blood direction (abluminal to luminal) by measuring the dpm for [^{14}C]-inulin and the cpm for the TCA-precipitable [^{125}I] radioactivity. The TQ of *Lrp1*$_{BE}^{-/-}$ brain endothelial cells was normalized to *Lrp1*$_{BE}^{fl/fl}$ brain endothelial cells. (**A**) Transport at a physiological concentration of 0.1 nM Aβ (*Lrp1*$_{BE}^{fl/fl}$, n = 18; *Lrp1*$_{BE}^{-/-}$, n = 14; 4 independent experiments). (**B**) Higher contribution of LRP1 in transport of [^{125}I] Aβ_{1-42} at higher Aβ concentrations (n = 6, n = 4, n = 5, n = 4, n = 3, n = 4, n = 3, n = 3 from left to right). Data represent mean ± SEM. For statistical analyses, unpaired t test was used. *P < 0.05, **P < 0.01, ***P < 0.001.

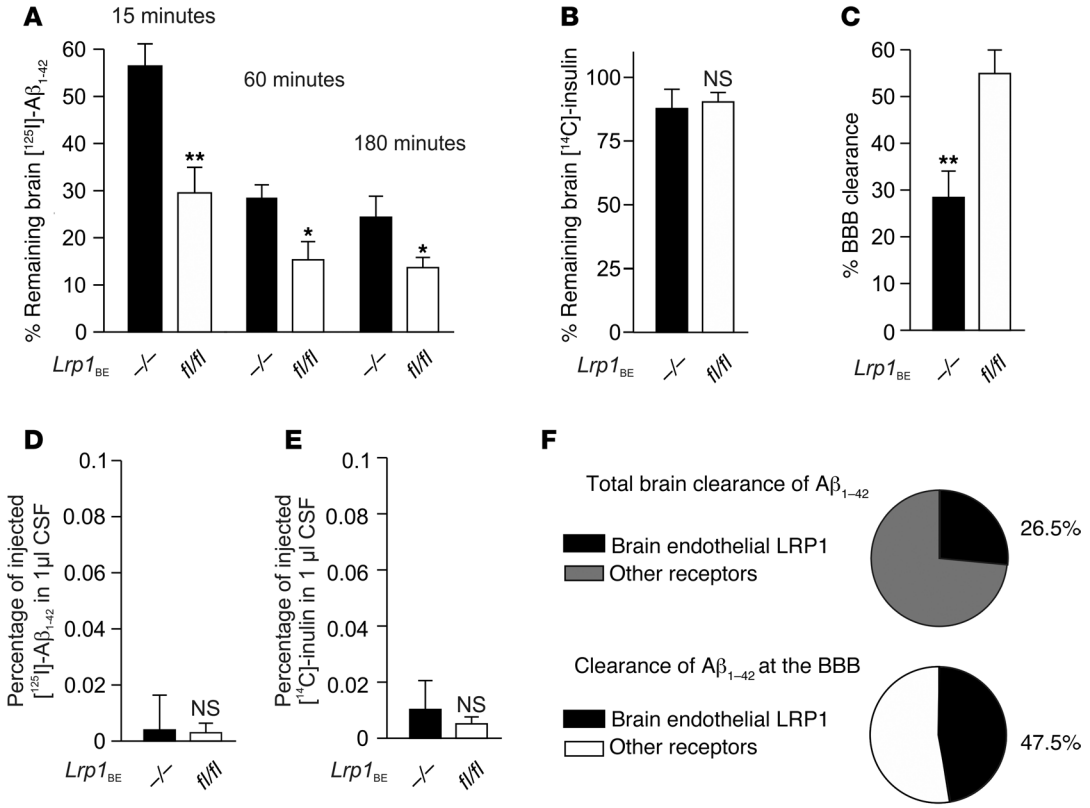

Figure 6. Brain endothelial LRP1 substantially mediates Aβ clearance in vivo. (**A**) 5.14 nM [^{125}I] $A\beta_{1-42}$ and 40 μCi/ml [^{14}C]-inulin, a paracellular marker, were microinfused into brain ISF of the caudate nucleus. Efflux was studied at designated time points by determining remaining radioactivity in the brain (n = 5, n = 5, n = 3, n = 3, n = 4, n = 5 mice per group from left to right). (**B**) No alteration was observed in the bulk flow clearance of [^{14}C]-inulin (n = 5 mice per group). (**C**) Efflux across the BBB of 5.14 nM [^{125}I] $A\beta_{1-42}$ 15 minutes after microinfusion in brain ISF demonstrated the substantial contribution of LRP1 (n = 5 mice per group). (**D** and **E**) Scarce presence of tracers in CSF 15 minutes after microinjection into the caudate nucleus (n = 3 mice per group). (**F**) Contribution of brain endothelial LRP1 to total and BBB clearance of 5.14 nM [^{125}I] $A\beta_{1-42}$ within 15 minutes (n = 5 mice per group). Data represent mean ± SEM. For statistical analyses, unpaired t test was used. *P < 0.05, **P < 0.01.

Here, in the two BBB-specific knockout mouse models of *Lrp1*, we can positively say that the expression of LRP1 in brain endothelial cells strongly modulates soluble brain Aβ levels.

$A\beta_{1-40}$ and $A\beta_{1-42}$ are the prevalent Aβ species found in amyloid plaques. In 7-month-old 5xFAD mice, we could not detect any significant differences in plaque deposition or gliosis when impairing a major Aβ elimination pathway through brain endothelial–specific deletion of *Lrp1*. However, absence of LRP1 in brain endothelium had striking effects on the concentrations of soluble Aβ species in the brain and resulted in significant cognitive deficits. As recent works suggest, the concentrations of soluble Aβ species, not the presence of plaques, seem to strongly correlate with the cognitive deficits in mouse models (54) and AD pathology in patients (55, 56). In their study with 19 patients with AD and 18 controls, McLean and colleagues discovered that insoluble Aβ in humans appeared only to signify the presence of AD and that soluble Aβ concentrations seemed to correlate with the severity of disease. Moreover, their data on patients with AD showed a higher proportion of $A\beta_{1-42}$ in the soluble fractions, possibly representing an intracellular and more neurotoxic pool of Aβ (55). In the AD mouse model, we could observe similar effects. Deleting *Lrp1* in brain endothelium severely increased soluble Aβ levels and elevated the $A\beta_{1-42}/A\beta_{1-40}$ ratio. This led to severe effects on cognitive function, supporting the idea that soluble Aβ, but not plaque-bound Aβ, correlates with AD-related symptoms.

It has been shown that LRP1 is required for APP trafficking and Aβ production. Inhibition of LRP1 in cultured cells has been shown to significant reduce Aβ production (57). In the 5xFAD model, these findings contradict the soluble Aβ accumulation that we observed in 5xFAD $Lrp1_{BE}^{-/-}$ mice. However, much of the Aβ in the brain is produced by neurons in which there is both high APP and LRP1 expression. LRP1 expression in neurons is not affected in this mouse model. The knockout of *Lrp1* is restricted to brain endothelium and choroid plexus epithelium. As endothelial cells constitute only 1% to 2% of all cells in the brain (58), we do not believe that in 5xFAD $Lrp1_{BE}^{-/-}$ mice there is a significant effect on APP trafficking and overall Aβ production in the brain, compared with that in 5xFAD $Lrp1_{BE}^{fl/fl}$ mice. Additionally, the results taken from the Aβ in vivo injection experiments in $Lrp1_{BE}^{-/-}$ mice are mirrored by these from the 5xFAD mice crossed into the $Lrp1_{BE}^{-/-}$ background. Therefore, we assume that the role of Aβ production in this paradigm is minimal.

In conclusion, the data gathered with the brain endothelial–specific *Lrp1* knockout mouse model prove that LRP1 in brain vasculature plays a key role in regulating brain Aβ levels. Although there are additional methods of Aβ clearance (6, 7, 38, 39), our and other data

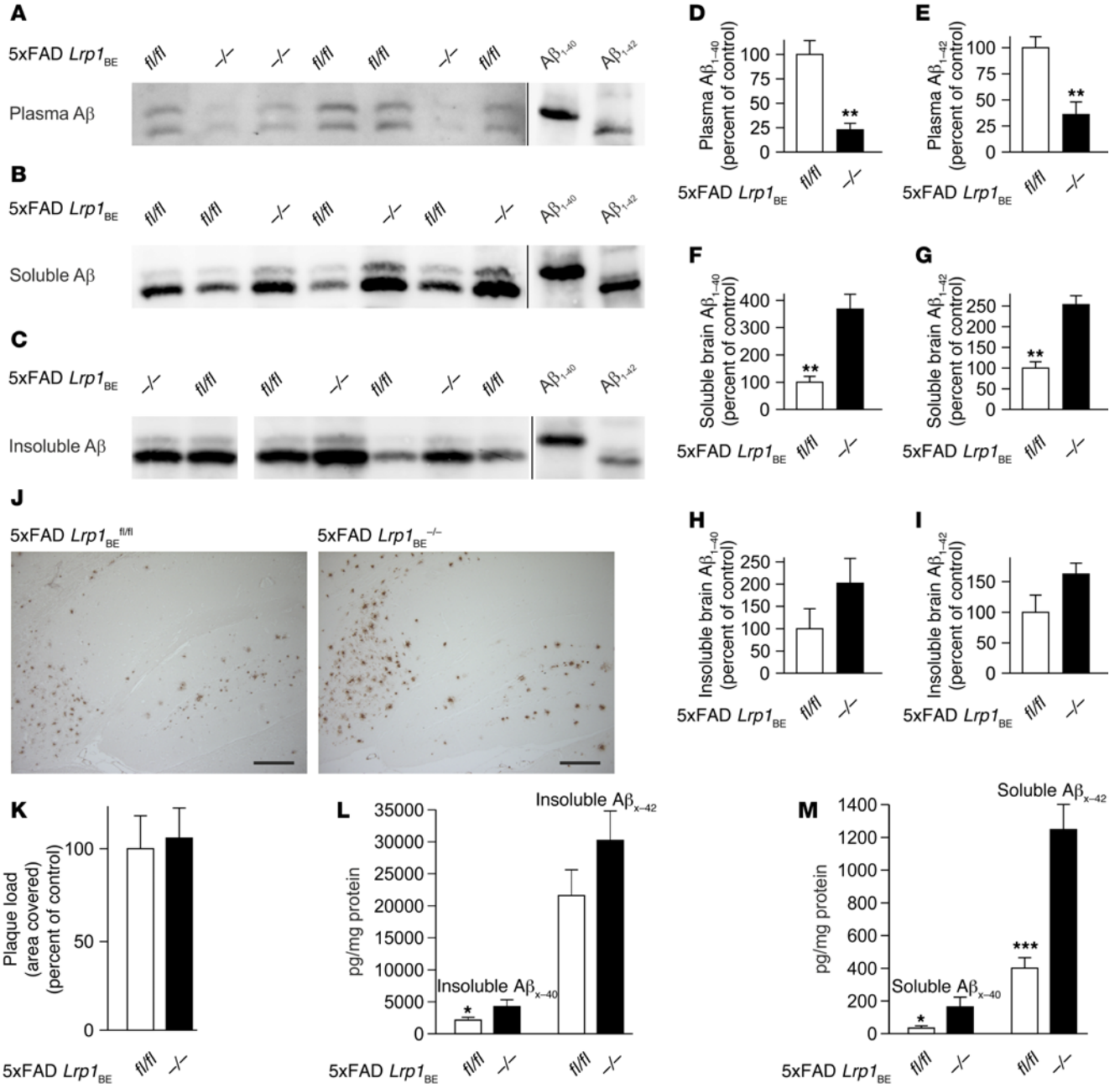

Figure 7. BBB clearance of Aβ species in 5xFAD mice is regulated by brain endothelial LRP1. Representative immunoprecipitations of (**A**) plasma Aβ, (**B**) soluble brain Aβ, and (**C**) insoluble brain Aβ, with 6E10 antibody from 7-month-old female mice show impaired brain-to-blood clearance of $Aβ_{1–40}$ and $Aβ_{1–42}$. Quantification of (**D**) plasma $Aβ_{1–40}$, (**E**) plasma $Aβ_{1–42}$, (**F**) soluble brain $Aβ_{1–40}$, (**G**) soluble brain $Aβ_{1–42}$, (**H**) insoluble brain $Aβ_{1–40}$, and (**I**) insoluble brain $Aβ_{1–42}$. $n = 3$ (**D** and **E**); $n = 4$ (**F** and **G**); $n = 5$ (*fl/fl*) and $n = 3$ (–/–) (**H** and **I**). (**J** and **K**) No effect on plaque deposition in hippocampus. $n = 5$ (*fl/fl*) and $n = 7$ (–/–) (**K**). Quantification of $Aβ_{x–40}$ and $Aβ_{x–42}$ using ELISA showed (**L**) insoluble and (**M**) significantly elevated soluble $Aβ_{x–40}$ and $Aβ_{x–42}$ levels in 7-month-old 5xFAD $Lrp1_{BE}^{-/-}$ mice. $n = 12$, $n = 5$, $n = 12$, $n = 5$ (**L**) and $n = 10$, $n = 5$, $n = 12$, $n = 5$ (**M**) from left to right. Data represent mean ± SEM of $n = 5$. All samples except for those shown in lanes 1 and 2 in **C** were analyzed on the same Western blot but rearranged for clearer presentation. A shorter exposure is shown for $Aβ_{1–40}$ and $Aβ_{1–42}$ standards in **A**. For statistical analyses, unpaired *t* test was used. $^*P < 0.05$, $^{**}P < 0.01$, $^{***}P < 0.001$. Scale bar: 200 μm.

show that vascular transport across the BBB is of crucial importance for rapid Aβ elimination from brain (8, 11, 15). Recent reports have identified different targets and strategies to restore and promote Aβ clearance at the BBB (16, 33, 59). As LRP1 levels decrease with aging and in AD, maintaining the function of Aβ transporters could be a potential strategy for treatment and prevention of AD.

Methods

Additional details are available in the Supplemental Methods.

Animals. Inducible *Lrp1* brain endothelial–specific knockout mice ($Lrp1_{BE}^{-/-}$) were generated by breeding $Lrp1^{fl/fl}$ mice (25) with *Slco1c1-CreER*^{T2} mice (24). To study Aβ transport without external invasion in vivo, we crossed $Lrp1_{BE}^{-/-}$ mice with 5xFAD mice, a

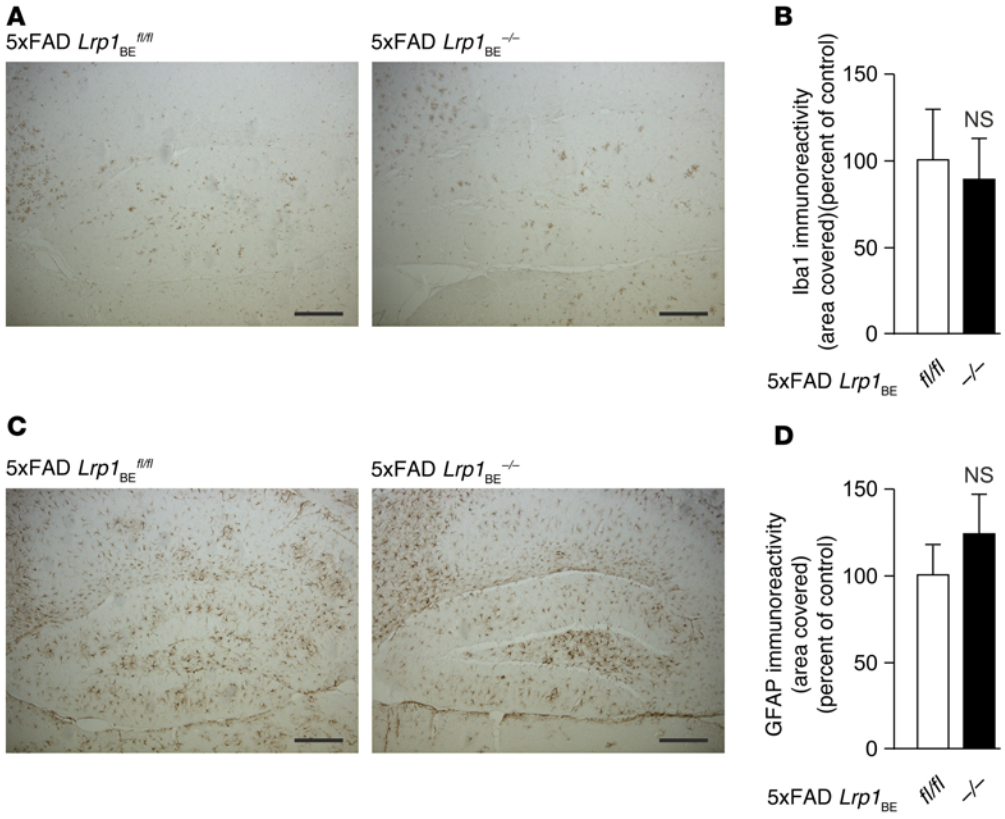

Figure 8. No difference in astrogliosis and microgliosis due to brain endothelial knockout of LRP1 in 5xFAD mice. Immunoreactivity for (**A** and **B**) Iba1 (microgliosis) and (**C** and **D**) GFAP (astrogliosis) in hippocampi of 5xFAD $Lrp1_{BE}^{-/-}$ (n = 5) and 5xFAD $Lrp1_{BE}^{fl/fl}$ (n = 7) mice (mean ± SEM). Representative results are shown in **A** and **C**. For statistical analyses, unpaired t test was used. Scale bar: 200 μm.

well-established AD model that harbors 3 *APP* mutations and 2 presenilin 1 mutations that are linked to FAD. Primers for genotyping are as follows: *Lrp1*-fwd, 5′-CATACCCTCTTCAAACCCCTTCCTG-3′ and *Lrp1*-rev, 5′-GCAAGCTCTCCTGCTCAGACCTGGA-3′ for loxP, *Cre*-fwd, 5′-GCTATTCATGTCTTGGAAGCC-3′ and *Cre*-rev, 5′-CAGGTTCTTCCTGACTTCATC-3′ for Cre; and 5xFAD-fwd 5′-CATGACCTGGGACATTCTC-3′ and 5xFAD-rev 5′-GTAGCAGAGGAGGAAGAAGTG-3′ for the 5xFAD site. Mice were housed on a 12-hour-light cycle. Unless stated otherwise, the animals had ad libitum access to water and a standard laboratory diet. In all experiments, littermates harboring ($Lrp1_{BE}^{-/-}$) or lacking ($Lrp1_{BE}^{fl/fl}$) the *Cre* allele were used. In order to induce recombination, 4- to 11-week-old mice were injected i.p. with 2 mg tamoxifen (T5648, Sigma-Aldrich) for 5 to 7 consecutive days. The analysis of recombination was examined 3 days after the last treatment. $Lrp1_{BE}^{fl/fl}$ control animals were treated equally. To maintain Cre-mediated recombination over time, 7-month-old animals were fed chow supplemented with 400 mg tamoxifen citrate per kilogram dry weight (CRE Active TAM400, LASvendi).

Reagents and antibodies. [^{125}I] $A\beta_{1-42}$ was purchased from Phoenix Peptide, and [^{14}C]-inulin was purchased from PerkinElmer. For a detailed description of all primary and secondary antibodies, see Supplemental Table 1.

Isolation of primary mouse brain capillary endothelial cells. Primary mouse brain capillary endothelial cells were isolated from 8- to 12-week-old littermate mice according to a standard protocol as described previously (32, 34). Cells were plated on 24-well Transwell filters (pore size, 0.4 μm; surface area, 33.6 mm^2; Greiner Bio-One) coated with collagen IV/fibronectin (Sigma-Aldrich). Cultures were maintained in DMEM supplemented with 20% plasma-derived bovine serum (First Link), 100 U/ml penicillin (Gibco), 100 μg/ml streptomycin (Gibco), 2 mM L-glutamine (Gibco), 4 μg/ml puromycin (Alexis), and 1 ng/ml FGF (R&D Systems) at 37°C and 5% CO_2. Cells were cultured in the cellZscope device, in which transendothelial electrical resistance (TEER) and capacitance were monitored over time. Puromycin was withdrawn after 4 days in culture. When cells reached confluency and the capacitance was around 1 μF/cm^2, culture medium was removed and serum-free DMEM/Ham's F12 (Gibco) medium containing 1 mM L-glutamine, 100 U/ml penicillin, and 100 μg/ml streptomycin was added. 550 nM hydrocortisone (Sigma-Aldrich) was supplemented to induce high TEER. The following day transport studies were performed.

Lysis of brain endothelial cells. For Western blot analysis, isolated primary cortical brain endothelial cells were solubilized in lysis buffer (50 mM TrisOH, 150 mM NaCl, 0.02% [w/v] NaN_3, 1% [v/v] Nonidet P-40 supplemented with a cocktail of phosphatase and proteinase inhibitors [PhosStop, Complete, Roche Applied Science]). Homogenates were centrifuged for 20 minutes at 15,000 g, and the supernatant was collected.

Analysis of recombination on DNA level. To analyze the efficiency of the tamoxifen-induced gene excision on DNA level, PCR analysis was performed using a PCR strategy with 3 primers to simultaneously detect WT, loxP flanked, and deleted *Lrp1* alleles (26). Genomic DNA was extracted from isolated primary cortical brain endothelial cells with the GenElute Mammalian Genomic DNA Miniprep Kit (Sigma-Aldrich) according to the manufacture's protocol. Three primers (A, 5′-TGGGATGAGGTAGACGCAGT-3′; B, 5′-CCTGGAGAACGTTCCAGTTC-3′; C, 5′-CCTGGAGAACGTTCCAGTTC-3′) were simultaneously used in one PCR reaction to investigate the efficiency

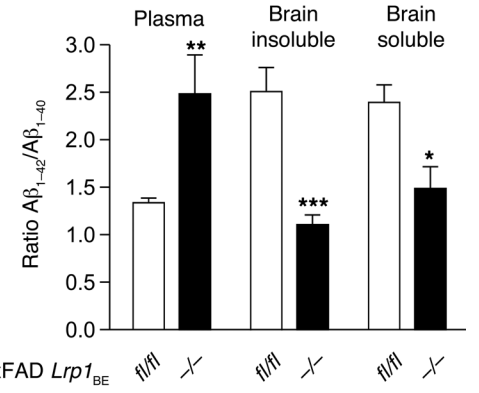

Figure 9. Preferential clearance of $A\beta_{1-40}$ species by brain endothelial LRP1. Contrasting the $A\beta_{1-42}/A\beta_{1-40}$ ratio in 5xFAD $Lrp1_{BE}^{-/-}$ and 5xFAD $Lrp1_{BE}^{fl/fl}$ Aβ pools demonstrates a differential clearance of Aβ species. Densitometry analysis of immunoprecipitated soluble brain Aβ, insoluble brain Aβ, and plasma Aβ with 6E10 antibody from 7-month-old mice (n = 3, n = 5, n = 7, n = 6, n = 3, n = 3 from left to right) showed higher $A\beta_{1-40}$ and $A\beta_{1-42}/A\beta_{1-40}$ ratios in plasma and lower and $A\beta_{1-42}/A\beta_{1-40}$ ratios in brain fractions when LRP1 is present in brain endothelial cells. Data represent mean ± SEM. For statistical analyses, unpaired t test was used. $^*P < 0.05$, $^{**}P < 0.01$, $^{***}P < 0.001$.

of the Cre-mediated recombination with regard to to the length of the different amplified products. Primers were designed to amplify a 541-bp product for the unexcised allele containing the loxP site, a 507-bp product for the WT allele, and a 325-bp product for the excised allele after Cre recombinase–catalyzed recombination.

Capillary depletion. Capillary-depleted brain homogenates were prepared as described elsewhere, using dextran density gradient centrifugation to separate microvessels from total brain homogenates (60).

Brain IgG extravasation. Levels of IgG in brains of $Lrp1_{BE}^{-/-}$ mice and controls at 36 weeks of age were evaluated by Western blotting. The mice were anesthetized with 125 mg/g pentobarbital and perfused transcardially with ice-cold PBS (137 mM NaCl, 2.7 mM KCl, 8.1 mM $Na_2HPO_4 \cdot 2H_2O$, 1.76 mM KH_2PO_4, pH 7.4). Brains were homogenized in lysis buffer (20 mM Tris-HCl [pH 7.5], 150 mM NaCl, 1 mM Na_2EDTA, 1 mM EGTA, 1% [v/v] Triton, 2.5 mM sodium pyrophosphate, 1 mM β-glycerophosphate, 1 mM Na_3VO_4, 1 μg/ml leupeptin, 1 mM phenylmethanesulfonylfluoride) on ice. The protein extracts were separated by SDS-PAGE, transferred onto nitrocellulose membranes (Amersham Hybond ECL), and then blocked in 5% (w/v) skim milk in TBST (20 mM Tris, 137 mM NaCl, 0.1% [v/v] Tween-20).

Brain fluorescein extravasation. BBB permeability was assessed with fluorescein extravasation in brains of $Lrp1_{BE}^{-/-}$ mice and controls at 36 weeks of age. The experiment was performed by administering mice 1.2 mg Na-fluorescein (Sigma-Aldrich) via retro-orbital intravenous injection under isoflurane anesthesia (5% in 70% N_2/30% 0_2). After 30 minutes, mice were anesthetized with pentobarbital 125 mg/g (w/w) and perfused transcardially with ice-cold PBS (137 mM NaCl, 2.7 mM KCl, 8.1 mM $Na_2HPO_4 \cdot 2H_2O$, 1.76 mM KH_2PO_4, pH 7.4) containing 10 IU/ml heparin. Brains were homogenized in 50 mM Tris-HCl, pH 8.0, and centrifuged at 16.1 g for 30 minutes. Supernatants were transferred to new tubes, and an equal volume absolute methanol was added. Samples were centrifuged at 16.1 g for 30 minutes, and the supernatant was transferred to a 96-well assay plate. A series of standards containing 0.001 to 10 μg/ml Na-fluorescein in 1:1 Tris-HCl/methanol (v/v) were added to each plate. The intensity of fluorescence was read at λ = 519 nm (excitation, 488 nm).

In vitro transcytosis of [^{125}I] $A\beta_{1-42}$. In order to study Aβ transcytosis in vitro, a standard transport model was used (5, 32, 34). [^{125}I] $A\beta_{1-42}$ (0.05 nM to 5 nM) and 1 μCi/ml [^{14}C]-inulin, a marker for paracellular diffusion, were added to serum-free media supplemented with 550 nM hydrocortisone and 40 mM HEPES and incubated at 37°C. To study blood-to-brain transport, 10 and 60 μl samples were taken from the luminal compartment after 45 minutes (0.1–5 nM [^{125}I] $A\beta_{1-42}$) or 90 minutes (0.05 nM [^{125}I] $A\beta_{1-42}$). The longer time period for the 0.05 nM [^{125}I] $A\beta_{1-42}$ concentration was necessary to be able to detect the amounts of transported protein. To investigate the amount of intact [^{125}I] $A\beta_{1-42}$ transported to the luminal side, 60 μl 15% TCA was added to a 60 μl luminal media sample and incubated for 10 minutes at 4°C. Samples were then centrifuged at 10,000 g for 10 minutes. Pellets (representing intact [^{125}I] $A\beta_{1-42}$) were counted for [^{125}I]. Transport of intact [^{125}I] $A\beta_{1-42}$ across the monolayer was calculated as $A\beta_{1-40}$ transcytosis quotient (TQ) using the following formula: $A\beta_{1-42}$ TQ = ([^{125}I] – $A\beta_{1-42}$ luminal/[^{125}I] – $A\beta_{1-42}$ input)/([^{14}C] – inulin acceptor/[^{14}C] – inulin input). Probes were counted on a Wallac Wizard2 2470 automatic γ-counter (PerkinElmer) for [^{125}I] or on a Tri-Carb 2800 TR Liquid Scintillation Analyser (PerkinElmer) for [^{14}C].

Brain efflux index method. A standard method was used to quantify brain-to-blood efflux rates (8, 11, 61). A stainless steel cannula was stereotaxically implanted into the right caudate putamen of age- and sex-matched mice that had been anesthetized with ketamine (800 mg/kg) and medetomidine (5 mg/kg). The cannula tip coordinates were as follows: 0.9 mm anterior from bregma, 1.9 mm lateral from midline, and 2.9 mm below the surface. Before injection of tracer molecules, animals recovered for 4 to 6 hours, a time point that precedes the start of the substantial inflammatory process, as assessed by histological analysis of tissue (negative staining for reactive astrocytes [GFAP] and reactive microglia [antiphosphotyrosine]), but allows partial BBB repair for large molecules, as reported previously (15, 61). 0.5 μl tracer fluid containing 1 μCi/ml [^{14}C]-inulin (reference marker) and physiological amounts of [^{125}I] $A\beta_{1-42}$ (5.14 nM) was injected with a 26-gauge needle attached to an UltraMicroPump controller (UMP3-1, Word Precision Instruments) into ISF over 5 minutes. After injection, the microsyringe was left in place for 5 minutes. Blinded brain samples were collected at different time points and prepared for analysis.

CSF isolation. 15 minutes after injection of tracers, as described above, 3.5- to 12-μl samples of CSF were taken from animals via cisterna magna puncture, as reported elsewhere (62), and used for radioactive analysis.

Calculation of in vivo [^{125}I] $A\beta_{1-42}$ clearance. In vivo [^{125}I] $A\beta_{1-42}$ clearance was calculated as reported before (8, 11, 15). The percentage of radioactivity remaining in the brain was calculated as follows: % recovery in brain = 100 × (N_b/N_i), where N_b is the radioactivity in the brain at the end of the experiment and N_i is the radioactivity injected into the brain, as illustrated by [^{14}C]-inulin (measured in dpm) and TCA-precipitable [^{125}I]-radioactivity (measured in cpm). The clearance rate for inulin, k_{inulin}, provides a measure of ISF flow, as inulin is neither transported across the BBB, nor retained in the brain (8). It is calculated as follows: $N_{b(inulin)}/N_{i(inulin)} = e^{-k_{inulin} \times t}$.

As previously reported, there are two major methods of Aβ elimination: direct transport across the BBB into the bloodstream and bulk

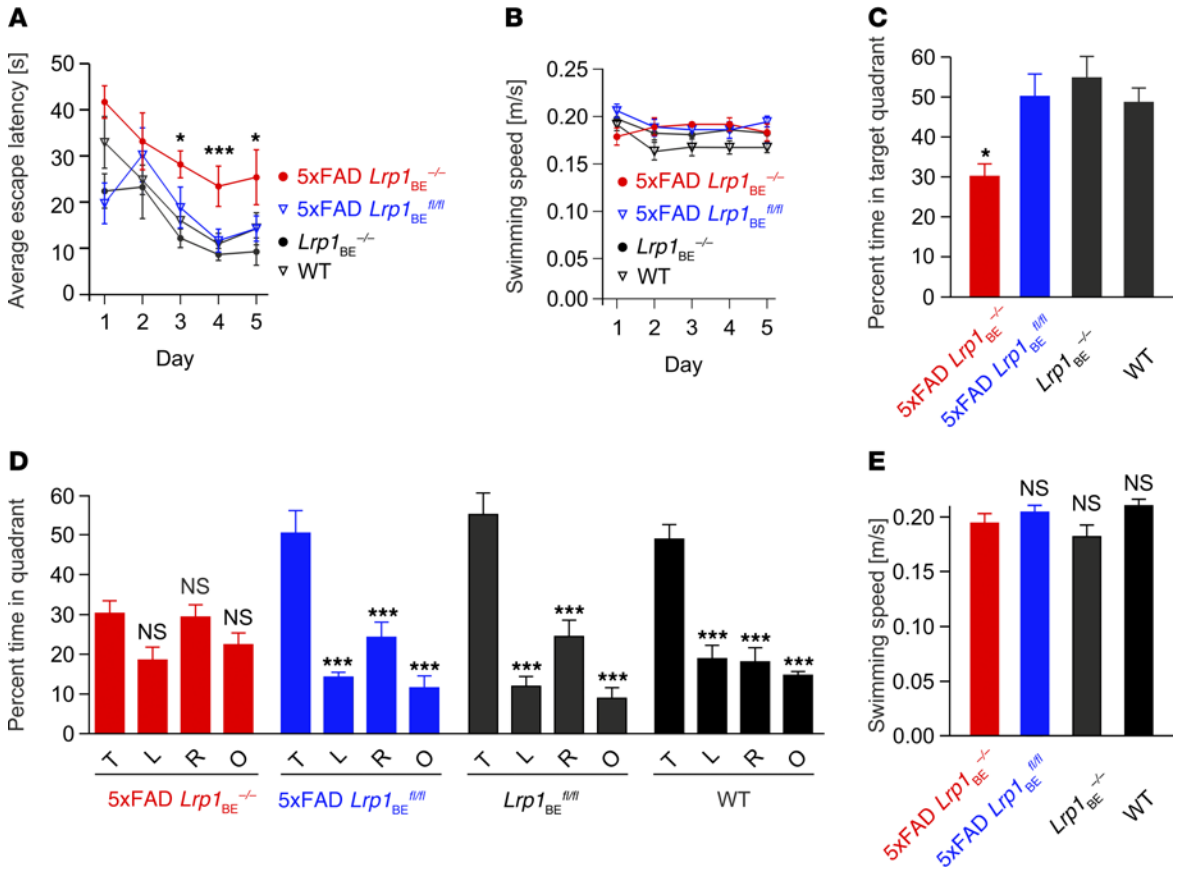

Figure 10. Deletion of *Lrp1* in brain endothelial cells leads to cognitive deficits in 5xFAD *Lrp1*$_{BE}^{-/-}$ mice. 7-month-old female 5xFAD *Lrp1*$_{BE}^{-/-}$ (n = 5), 5xFAD *Lrp1*$_{BE}^{fl/fl}$ (n = 7), *Lrp1*$_{BE}^{-/-}$ (n = 5), and WT (n = 6) control mice were tested. (**A**) Animals underwent acquisition training to learn to use proximal and distal cues to navigate a path to a hidden platform. A significant difference in the escape latency of 5xFAD *Lrp1*$_{BE}^{-/-}$ mice compared with that of all other groups was seen on days 3 to 5. (**B** and **E**) Swimming speed was not affected in all mice tested. (**C**) Spatial reference memory deficits in 5xFAD *Lrp1*$_{BE}^{-/-}$ mice were shown in the probe trial, in which 5xFAD *Lrp1*$_{BE}^{-/-}$ mice spent significantly less time in the target quadrant than all other groups of mice. The probe trial was given after the acquisition training phase to assess spatial reference memory. (**D**) 5xFAD *Lrp1*$_{BE}^{fl/fl}$ mice showed no impairment of spatial reference memory, as reflected by the significant greater percentage of time spent in the target quadrant ($P < 0.001$ target vs. left, right, and opposite quadrant). The probe trial revealed a significant impairment of spatial reference memory in 5xFAD *Lrp1*$_{BE}^{-/-}$ mice, as they showed no preference for the target quadrant. T, target quadrant; L, left quadrant; R, right quadrant; O, opposite quadrant. Data represent mean ± SEM. For statistical analyses, the following test was used: repeated-measures ANOVA followed by Bonferroni multiple comparisons. *$P < 0.05$, ***$P < 0.001$.

flow clearance. In addition, Aβ can be retained in the brain by binding to transport proteins or cell-surface receptors (8).

According to our model, the fraction of Aβ remaining in the brain can be expressed as follows: $N_{b(A\beta)}/N_{i(A\beta)} = (a_1 + a_2) \times e^{-(k1+k2) \times t}$, where $a_1 = k_2/(k_1+k_2)$, $a_2 = (1 - (k_2/(k_1 + k_2)))$, k_1 signifies the total efflux, and k_2 represents the retention in the brain.

Clearance of [^{125}I] $A\beta_{1-42}$ via the BBB was calculated as $[(1 - N_{b(A\beta)}/N_{b(A\beta)} - (1 - N_{b(inulin)}/N_{b(inulin)})] \times 100$ using a standard time of 15 minutes where efflux was linear. Clearance of brain endothelial LRP1 was calculated by subtracting BBB-mediated clearance of *Lrp1*$_{BE}^{-/-}$ mice from *Lrp1*$_{BE}^{fl/fl}$ mice.

Measurement of Aβ species by ELISA. Brains were weighed and subjected to a sequential Aβ extraction. Then, brains were homogenized in PBS containing complete protease and phosphatase inhibitor (Roche Applied Science) using a glass homogenizer and subsequently centrifuged at 55,000 *g* for 20 minutes at 4°C. The supernatant, containing soluble brain Aβ, was removed and stored at –80°C. Then, the pellet was dissolved in 2% SDS in PBS containing complete protease and phosphatase inhibitor, sonificated, incubated for 30 minutes on ice, and centrifuged at 55,000 *g* for 20 minutes at 4°C. Supernatants, containing insoluble plaque-associated Aβ, were immediately frozen at –80°C.

The levels of $A\beta_{x-40}$ and $A\beta_{x-42}$ peptides in brain extractions were blindly determined using a cell-based sandwich ELISA assay as described previously (63).

Immunoprecipitation of Aβ. Total Aβ was immunoprecipitated from blinded samples of blood serum and soluble and insoluble brain pools by mixing 5-fold concentrated detergent buffer (50 mM HEPES [pH 7.4], 150 mM NaCl, 0.5 % [v/v] Nonidet P-40, 0.05% [w/v] SDS and protease inhibitor cocktail [Roche Applied Science]) with the respective samples. Magnetic Dynabeads (M-280 Sheep Anti-Mouse IgG, 11201D, Novex) containing sheep anti-mouse IgG attached to their surface were precoated with 6E10 antibody (Covance) according to the manufacturer's protocols and added to the samples. After overnight incubation at 4°C, samples were washed 3 times in PBS, 0.1% (w/v) BSA, and once in 10 mM Tris-HCl, pH 7.5. After heating the samples to 95°C in 25-μl sample buffer (0.36 M Bis-Tris, 0.16 M bicine, 1% [w/v] SDS, 15% [w/v] sucrose, and 0.0075% [w/v] bromphenol blue) the supernatants were subjected to PAGE.

Aβ separation with 8 M urea SDS gel and Western blotting. Separation of immunoprecipitated Aβ peptides was performed together with peptide standards on 0.75-mm 10% T/5% C polyacrylamide 8 M urea SDS gels. For separation of $Aβ_{1-40}$ from $Aβ_{1-42}$, a final concentration of 0.3 M H_2SO_4 was used in resolving gels. Peptides were transferred to an Immobilion-P PVDF membrane via semi-dry Western blotting (Bio-Rad) at 46 mA for 45 minutes. Membranes were boiled for 3 minutes in PBS and blocked in 5% skim milk in TBST (20 mM Tris, 137 mM NaCl, 0.1% [v/v] Tween-20) for 30 minutes afterward.

Immunohistochemistry and immunocytochemistry. 8-μm frozen sections of perfused mouse brains or isolated cells were fixed in ice-cold methanol for 30 minutes. Unspecific binding sites were blocked using a solution of 10% (v/v) goat serum and 1% (w/v) BSA in PBS. Unconjugated chicken anti-mouse IgG (SAB3701114, Sigma-Aldrich) was used to block endogenous mouse IgG. Sections were incubated in primary antibody solution at 37°C for 1 hour, washed, and incubated at room temperature with secondary antibodies for 90 minutes. For some experiments, cell nuclei were stained with DRAQ5 (Biostatus Limited) in PBS for 10 minutes at room temperature. Samples were embedded in Prolong Gold Antifade Reagent (Invitrogen), dried overnight at room temperature, and analyzed with a confocal laser scanning microscope. Stainings were documented with a LSM710 microscope (Zeiss) equipped with ZEN 2011 SP2 software.

Paraffin sections were stained as described previously (64). Images were obtained using an Olympus BX-51 microscope equipped with a DP-50 camera (Olympus).

Quantification of plaque load, astrogliosis, and microgliosis. Plaque load quantification was performed as described previously (65). For quantification of astrogliosis and microgliosis, sections were stained with anti-GFAP and anti-IBA1 and analyzed likewise. Three sections per animal were analyzed.

Chemiluminescence detection. Signal detection in all Western blotting experiments was carried out using HRP-conjugated secondary antibodies and ELC assay solutions (Millipore and Thermo Scientific Pierce) and LAS-3000 mini (Fujifilm). Western blots signals were quantified using NIH ImageJ (version 1.44).

Generation of monoclonal 11E2 anti-LRP1. Monoclonal 11E2 was generated as described previously (66). Briefly, *Prnp* knockout mice were immunized with purified LRP1 ligand–binding domains II and IV, and a fusion to generate hybridoma was performed according to standard protocols (66). Screening of hybridoma supernatants was done using dot blot and Western blot to detect the immunogen.

Spatial learning and spatial reference memory assessed by Morris water maze. The ability of vision of the mice was tested by visual placing (42) before mice entered the Morris water maze. Spatial reference memory in 5xFAD $Lrp1_{BE}^{-/-}$ mice and 5xFAD $Lrp1_{BE}^{fl/fl}$ control mice was assessed using the Morris water maze (40) by a blinded investigator as described previously (41). In brief, mice learn to locate a hidden platform in a circular pool filled with opaque water. The pool was divided into 4 virtual quadrants that were defined based on their spatial relationship to the platform: left, right, opposite, and target quadrant, which contained the goal platform. ANY-Maze video-tracking software (Stoelting Co.) was used to record escape latency, swimming speed, and quadrant preference. 7-month-old female 5xFAD $Lrp1_{BE}^{-/-}$ ($n = 7$), 5xFAD $Lrp1_{BE}^{fl/fl}$ ($n = 7$), $Lrp1_{BE}^{-/-}$ ($n = 5$), and WT ($n = 6$) control mice were tested.

The experiment began with 3 days of cued training, during which the platform was marked with a triangular flag. Both the location of the platform and the position from where the mice were introduced into the pool changed between trials. Each mouse received 4 training trials per day with an average intertrial interval of 15 minutes.

24 hours after the last day of cued training, mice performed 5 days of acquisition training. For this the flag was removed from the platform. In addition to distal cues existing in the room, proximal cues were attached to the outside of the pool. The platform position remained stationary for each mouse throughout training. Trials were conducted as they were during the cued training phase.

24 hours after the last acquisition trial, a probe test was performed to analyze spatial reference memory. The platform was removed, and mice were introduced into the water from a novel entry point. Mice were allowed to swim freely for 1 minute while their swimming path was recorded. After the probe trial, mice were sacrificed.

Statistics. Statistical analysis was performed using GraphPad Prism software (version 5, GraphPad Software). Unpaired 2-tailed *t* tests and 1-way ANOVA followed by Bonferroni multiple comparisons were used. Statistical significance was defined as $P < 0.05$.

Study approval. All animal studies were conducted in compliance with European and German guidelines for the care and use of laboratory animals and were approved by the Central Animal Facility of the University of Mainz and the ethical committee on animal care and use of Rhineland-Palatinate, Germany.

Author contributions

SES designed the studies, performed the majority of experiments, analyzed data, and wrote the manuscript. SM performed experiments and contributed to the experimental design and the writing of the manuscript. AH contributed to the experimental design. JN and SB performed experiments. JNM, NS, and ADS performed experiments and contributed to the writing of the manuscript. REV and YB contributed to experimental design, performed experiments, and analyzed data. CK supervised the experimental design. SW, MS, and TAB supervised the experimental design and contributed to the writing of the manuscript. CUP designed the studies and supervised the experimental design and the entire work of the manuscript. All authors discussed the results, read, and approved the final manuscript.

Acknowledgments

We thank Roswitha Nehrbaß for excellent technical assistance. S.E. Storck would like to thank Michael Meister for assistance with mathematical modeling. In addition, we would like to thank Joachim Herz for providing $Lrp1^{fl/fl}$ mice. Parts of this work were supported by the Stiftung Rheinland Pfalz and the Deutsche Forschungsgemeinschaft (PI 379/8-1 to C.U. Pietrzik) and by the Competence Network Degenerative Dementias of the Federal Ministry of Education (to C.U. Pietrzik and T.A. Bayer). We thank Karlheinz Baumann and Manfred Brockhaus (F. Hoffmann–La Roche Ltd., Switzerland) for carboxyl-terminus–specific Aβ antibodies.

Address correspondence to: Claus U. Pietrzik, University Medical Center of Johannes Gutenberg University Mainz, Institute for Pathobiochemistry, Molecular Neurodegeneration, Duesbergweg 6, 55099 Mainz, Germany. Phone: 49.6131.39.25390; E-mail: pietrzik@uni-mainz.de.

1. Mawuenyega KG, et al. Decreased clearance of CNS β-amyloid in Alzheimer's disease. *Science*. 2010;330(6012):1774.
2. Naslund J, et al. Relative abundance of Alzheimer Aβ amyloid peptide variants in Alzheimer disease and normal aging. *Proc Natl Acad Sci U S A*. 1994;91(18):8378–8382.
3. Zlokovic BV. Neurovascular mechanisms of Alzheimer's neurodegeneration. *Trends Neurosci*. 2005;28(4):202–208.
4. Tarasoff-Conway JM, et al. Clearance systems in the brain-implications for Alzheimer disease. *Nat Rev Neurol*. 2015;11(8):457–470.
5. Nazer B, Hong S, Selkoe DJ. LRP promotes endocytosis and degradation, but not transcytosis, of the amyloid-β peptide in a blood-brain barrier in vitro model. *Neurobiol Dis*. 2008;30(1):94–102.
6. Kanekiyo T, et al. Neuronal clearance of amyloid-β by endocytic receptor LRP1. *J Neurosci*. 2013;33(49):19276–19283.
7. Kanekiyo T, Liu CC, Shinohara M, Li J, Bu G. LRP1 in brain vascular smooth muscle cells mediates local clearance of Alzheimer's amyloid-β. *J Neurosci*. 2012;32(46):16458–16465.
8. Shibata M, et al. Clearance of Alzheimer's amyloid-ss(1-40) peptide from brain by LDL receptor-related protein-1 at the blood-brain barrier. *J Clin Invest*. 2000;106(12):1489–1499.
9. Silverberg GD, et al. Amyloid efflux transporter expression at the blood-brain barrier declines in normal aging. *J Neuropathol Exp Neurol*. 2010;69(10):1034–1043.
10. Kang DE, et al. Modulation of amyloid β-protein clearance and Alzheimer's disease susceptibility by the LDL receptor-related protein pathway. *J Clin Invest*. 2000;106(9):1159–1166.
11. Bell RD, et al. Transport pathways for clearance of human Alzheimer's amyloid β-peptide and apolipoproteins E and J in the mouse central nervous system. *J Cereb Blood Flow Metab*. 2007;27(5):909–918.
12. Deane R, et al. apoE Isoform-specific disruption of amyloid β peptide clearance from mouse brain. *J Clin Invest*. 2008;118(12):4002–4013.
13. Zhao Z, et al. Central role for PICALM in amyloid-β blood-brain barrier transcytosis and clearance. *Nat Neurosci*. 2015;18(7):978–987.
14. Rebeck GW, Harr SD, Strickland DK, Hyman BT. Multiple, diverse senile plaque-associated proteins are ligands of an apolipoprotein E receptor, the α2-macroglobulin receptor/low-density-lipoprotein receptor-related protein. *Ann Neurol*. 1995;37(2):211–217.
15. Deane R, Wu Z, Zlokovic BV. RAGE (yin) versus LRP (yang) balance regulates alzheimer amyloid beta-peptide clearance through transport across the blood-brain barrier. *Stroke*. 2004;35(11 suppl 1):2628–2631.
16. Roberts KF, et al. Amyloid-β efflux from the CNS into the plasma. *Ann Neurol*. 2014;76(6):837–844.
17. Ito S, Ueno T, Ohtsuki S, Terasaki T. Lack of brain-to-blood efflux transport activity of low-density lipoprotein receptor-related protein-1 (LRP-1) for amyloid-β peptide(1-40) in mouse: involvement of an LRP-1-independent pathway. *J Neurochem*. 2010;113(5):1356–1363.
18. Ito S, Ohtsuki S, Kamiie J, Nezu Y, Terasaki T. Cerebral clearance of human amyloid-beta peptide (1-40) across the blood-brain barrier is reduced by self-aggregation and formation of low-density lipoprotein receptor-related protein-1 ligand complexes. *J Neurochem*. 2007;103(6):2482–2490.
19. Yamada K, et al. The low density lipoprotein receptor-related protein 1 mediates uptake of amyloid β peptides in an in vitro model of the blood-brain barrier cells. *J Biol Chem*. 2008;283(50):34554–34562.
20. Candela P, et al. In vitro discrimination of the role of LRP1 at the BBB cellular level: focus on brain capillary endothelial cells and brain pericytes. *Brain Res*. 2015;1594:15–26.
21. Qosa H, et al. Differences in amyloid-β clearance across mouse and human blood-brain barrier models: kinetic analysis and mechanistic modeling. *Neuropharmacology*. 2014;79:668–678.
22. Herz J, Clouthier DE, Hammer RE. LDL receptor-related protein internalizes and degrades uPA-PAI-1 complexes and is essential for embryo implantation. *Cell*. 1992;71(3):411–421.
23. Herz J, Couthier DE, Hammer RE. Correction: LDL receptor-related protein internalizes and degrades uPA-PAI-1 complexes and is essential for embryo implantation. *Cell*. 1993;73(3):428.
24. Ridder DA, et al. TAK1 in brain endothelial cells mediates fever and lethargy. *J Exp Med*. 2011;208(13):2615–2623.
25. Rohlmann A, Gotthardt M, Hammer RE, Herz J. Inducible inactivation of hepatic LRP gene by cre-mediated recombination confirms role of LRP in clearance of chylomicron remnants. *J Clin Invest*. 1998;101(3):689–695.
26. Leneuve P, Zaoui R, Monget P, Le Bouc Y, Holzenberger M. Genotyping of Cre-lox mice and detection of tissue-specific recombination by multiplex PCR. *Biotechniques*. 2001;31(5):1156–1160.
27. Bu G, Maksymovitch EA, Nerbonne JM, Schwartz AL. Expression and function of the low density lipoprotein receptor-related protein (LRP) in mammalian central neurons. *J Biol Chem*. 1994;269(28):18521–18528.
28. Lillis AP, Van Duyn LB, Murphy-Ullrich JE, Strickland DK. LDL receptor-related protein 1: unique tissue-specific functions revealed by selective gene knockout studies. *Physiol Rev*. 2008;88(3):887–918.
29. Wolf BB, Lopes MB, VandenBerg SR, Gonias SL. Characterization and immunohistochemical localization of α2-macroglobulin receptor (low-density lipoprotein receptor-related protein) in human brain. *Am J Pathol*. 1992;141(1):37–42.
30. Tooyama I, et al. Subcellular localization of the low density lipoprotein receptor-related protein (α2-macroglobulin receptor) in human brain. *Brain Res*. 1995;691(1–2):235–238.
31. Tooyama I, Kawamata T, Akiyama H, Moestrup SK, Gliemann J, McGeer PL. Immunohistochemical study of α2 macroglobulin receptor in Alzheimer and control postmortem human brain. *Mol Chem Neuropathol*. 1993;18(1–2):153–160.
32. Pflanzner T, et al. LRP1 mediates bidirectional transcytosis of amyloid-β across the blood-brain barrier. *Neurobiol Aging*. 2011;32(12):2323 e1–2323 11.
33. Qosa H, Abuznait AH, Hill RA, Kaddoumi A. Enhanced brain amyloid-β clearance by rifampicin and caffeine as a possible protective mechanism against Alzheimer's disease. *J Alzheimers Dis*. 2012;31(1):151–165.
34. Pflanzner T, et al. Cellular prion protein participates in amyloid-β transcytosis across the blood-brain barrier. *J Cereb Blood Flow Metab*. 2012;32(4):628–632.
35. Li Y, Lu W, Marzolo MP, Bu G. Differential functions of members of the low density lipoprotein receptor family suggested by their distinct endocytosis rates. *J Biol Chem*. 2001;276(21):18000–18006.
36. Davis J, et al. Early-onset and robust cerebral microvascular accumulation of amyloid β-protein in transgenic mice expressing low levels of a vasculotropic Dutch/Iowa mutant form of amyloid β-protein precursor. *J Biol Chem*. 2004;279(19):20296–20306.
37. Oakley H, et al. Intraneuronal β-amyloid aggregates, neurodegeneration, and neuron loss in transgenic mice with five familial Alzheimer's disease mutations: potential factors in amyloid plaque formation. *J Neurosci*. 2006;26(40):10129–10140.
38. Wyss-Coray T, et al. TGF-β1 promotes microglial amyloid-beta clearance and reduces plaque burden in transgenic mice. *Nat Med*. 2001;7(5):612–618.
39. Wyss-Coray T, et al. Adult mouse astrocytes degrade amyloid-beta in vitro and in situ. *Nat Med*. 2003;9(4):453–457.
40. Morris R. Developments of a water-maze procedure for studying spatial learning in the rat. *J Neurosci Methods*. 1984;11(1):47–60.
41. Bouter Y, et al. N-truncated amyloid beta (Aβ) 4-42 forms stable aggregates and induces acute and long-lasting behavioral deficits. *Acta Neuropathol*. 2013;126(2):189–205.
42. Heyser CJ. Assessment of developmental milestones in rodents. *Curr Protoc Neurosci*. 2004;Chapter 8:Unit 8.18.
43. Bouter Y, et al. Deciphering the molecular profile of plaques, memory decline and neuron loss in two mouse models for Alzheimer's disease by deep sequencing. *Front Aging Neurosci*. 2014;6:75.
44. de la Torre JC. Alzheimer disease as a vascular disorder: nosological evidence. *Stroke*. 2002;33(4):1152–1162.
45. Iadecola C. Neurovascular regulation in the normal brain and in Alzheimer's disease. *Nat Rev Neurosci*. 2004;5(5):347–360.
46. Pi X, et al. LRP1-dependent endocytic mechanism governs the signaling output of the bmp system in endothelial cells and in angiogenesis. *Circ Res*. 2012;111(5):564–574.
47. Pflanzner T, Kuhlmann CR, Pietrzik CU. Blood-brain-barrier models for the investigation of transporter- and receptor-mediated amyloid-β clearance in Alzheimer's disease. *Curr Alzheimer Res*. 2010;7(7):578–590.
48. Wang X, et al. Lipoprotein receptor-mediated induction of matrix metalloproteinase by tissue plasminogen activator. *Nat Med*. 2003;9(10):1313–1317.
49. Kanekiyo T, Bu G. The low-density lipoprotein receptor-related protein 1 and amyloid-β clearance in Alzheimer's disease. *Front Aging Neurosci*.

2014;6:93.
50. Deane R, et al. LRP/amyloid β-peptide interaction mediates differential brain efflux of Aβ isoforms. *Neuron*. 2004;43(3):333–344.
51. Sagare A, et al. Clearance of amyloid-β by circulating lipoprotein receptors. *Nat Med*. 2007;13(9):1029–1031.
52. Ito S, Ohtsuki S, Terasaki T. Functional characterization of the brain-to-blood efflux clearance of human amyloid-β peptide (1-40) across the rat blood-brain barrier. *Neurosci Res*. 2006;56(3):246–252.
53. Tuma P, Hubbard AL. Transcytosis: crossing cellular barriers. *Physiol Rev*. 2003;83(3):871–932.
54. Dodart JC, et al. Immunization reverses memory deficits without reducing brain Aβ burden in Alzheimer's disease model. *Nat Neurosci*. 2002;5(5):452–457.
55. McLean CA, et al. Soluble pool of Aβ amyloid as a determinant of severity of neurodegeneration in Alzheimer's disease. *Ann Neurol*. 1999;46(6):860–866.
56. Mc Donald JM, et al. The presence of sodium dodecyl sulphate-stable Aβ dimers is strongly associated with Alzheimer-type dementia. *Brain*. 2010;133(pt 5):1328–1341.
57. Ulery PG, et al. Modulation of β-amyloid precursor protein processing by the low density lipoprotein receptor-related protein (LRP). Evidence that LRP contributes to the pathogenesis of Alzheimer's disease. *J Biol Chem*. 2000;275(10):7410–7415.
58. van Beijnum JR, Rousch M, Castermans K, van der Linden E, Griffioen AW. Isolation of endothelial cells from fresh tissues. *Nat Protoc*. 2008;3(6):1085–1091.
59. Deane R, et al. A multimodal RAGE-specific inhibitor reduces amyloid β-mediated brain disorder in a mouse model of Alzheimer disease. *J Clin Invest*. 2012;122(4):1377–1392.
60. Deane R, Zheng W, Zlokovic BV. Brain capillary endothelium and choroid plexus epithelium regulate transport of transferrin-bound and free iron into the rat brain. *J Neurochem*. 2004;88(4):813–820.
61. Cirrito JR, et al. P-glycoprotein deficiency at the blood-brain barrier increases amyloid-β deposition in an Alzheimer disease mouse model. *J Clin Invest*. 2005;115(11):3285–3290.
62. Vandenbroucke RE, et al. Matrix metalloprotease 8-dependent extracellular matrix cleavage at the blood-CSF barrier contributes to lethality during systemic inflammatory diseases. *J Neurosci*. 2012;32(29):9805–9816.
63. Hahn S, et al. Presenilin-1 but not amyloid precursor protein mutations present in mouse models of Alzheimer's disease attenuate the response of cultured cells to γ-secretase modulators regardless of their potency and structure. *J Neurochem*. 2011;116(3):385–395.
64. Wirths O, et al. Pyroglutamate Aβ pathology in APP/PS1KI mice, sporadic and familial Alzheimer's disease cases. *J Neural Transm*. 2010;117(1):85–96.
65. Wittnam JL, et al. Pyroglutamate amyloid beta (Aβ) aggravates behavioral deficits in transgenic amyloid mouse model for Alzheimer disease. *J Biol Chem*. 2012;287(11):8154–8162.
66. Korth C, Streit P, Oesch B. Monoclonal antibodies specific for the native, disease-associated isoform of the prion protein. *Methods Enzymol*. 1999;309:106–122.